

Soft Matter

Accepted Manuscript

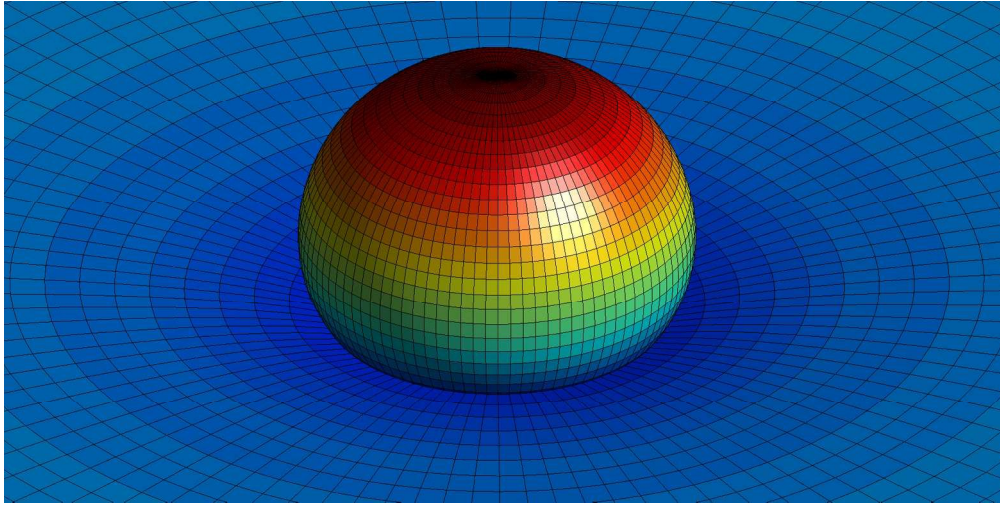


This is an *Accepted Manuscript*, which has been through the Royal Society of Chemistry peer review process and has been accepted for publication.

Accepted Manuscripts are published online shortly after acceptance, before technical editing, formatting and proof reading. Using this free service, authors can make their results available to the community, in citable form, before we publish the edited article. We will replace this *Accepted Manuscript* with the edited and formatted *Advance Article* as soon as it is available.

You can find more information about *Accepted Manuscripts* in the [Information for Authors](#).

Please note that technical editing may introduce minor changes to the text and/or graphics, which may alter content. The journal's standard [Terms & Conditions](#) and the [Ethical guidelines](#) still apply. In no event shall the Royal Society of Chemistry be held responsible for any errors or omissions in this *Accepted Manuscript* or any consequences arising from the use of any information it contains.



Graphical Abstract

We report the analytical and experimental characterisation of the deformation of a liquid marble floating on a liquid surface.

ARTICLE

Deformation of a floating liquid marble

Chin Hong Ooi,^a Raja Vadivelu,^b James St John,^b Dzung Viet Dao,^a Nam-Trung Nguyen,^{a*}

fCite this: DOI:
10.1039/x0xx00000x

Received 00th January 2012,
Accepted 00th January 2012

DOI: 10.1039/x0xx00000x

www.rsc.org/

A rigid spherical particle floating on a liquid is a known problem with well-defined solutions. Under the combined effect of gravity and surface tension, the rigid particle deforms the liquid surface. However, in the case of a floating soft particle such as a liquid marble, not only the liquid surface but also the particle itself deform. In this paper, we investigate the deformation of a floating liquid marble and characterise its height as well as aspect ratio. The experimental results show that theoretical models for a rigid spherical particle suit well for small liquid marbles. Larger marbles require an oblate liquid spheroid model. We will discuss the limitations of the two models and characterise the deformation of these marbles.

1. Introduction

Archimedes principle applies to a floating object stating that the buoyancy force is equal to the weight of the liquid volume displaced by the submerged volume of the object. This principle does not take into account the surface tension forces of the liquid surface, which are usually neglected for large objects. For smaller objects however, surface tension plays a dominant role over buoyancy force. It is well known that objects even denser than water such as a metal paper clip can actually float on water surface. In nature, water striders skid across water surface with ease. Various research groups have investigated these phenomena in great details. The knowledge gained from this research has been exploited for various applications such as filtering of ore and sorting of biochemical material.

A liquid marble is a liquid droplet coated with a layer of hydrophobic powder which can also float on a liquid surface. Bormashenko *et al.* floated brine liquid marbles coated with polyvinylidene fluoride (PVDF) nanobeads on water and determined the maximum density before it sank.¹ The approach of this work is similar to that reported by Vella *et al.*, where the critical maximum density of a floating solid object was investigated.² There are a few key differences between a floating liquid marble and a floating solid object. Unlike a solid object, a layer of air gap exists between the liquid marble coating and the carrier liquid.^{3,4} This air gap prevents the direct contact between the liquids inside and outside of the marble. For miscible liquid droplets, the air gap can be formed by bouncing the droplet on the liquid surface.⁵

Due to the hydrophobic nature of the liquid marble coating, a large contact angle is formed similar to the Cassie-Baxter⁶ or Extrand⁷ rough surface configuration. Dupin *et al.*⁸ and Fujii *et al.*⁹ used latex-based coatings to float a liquid marble which is responsive to pH changes in the carrier liquid. Oligomeric and polymeric tetrafluoroethylene have been used to float ionic liquid marbles.¹⁰ Zhang *et al.* used a magnet to move a liquid marble with a hydrophobised iron oxide-based coating.¹¹ Instead of water, Bormashenko *et al.* used organic liquid as the carrier.¹² These previous works demonstrated that liquid marbles could sink intact, similar to a Pickering emulsion.

To the best knowledge of the authors, none of the reported studies conducted any quantitative study on the mechanisms of liquid marble floating and moving on another liquid. As the liquid marble is porous, gas exchange is permitted between the liquid content and its surrounding without any direct liquid contact. This property is very useful for biomedical applications such as aerobic cell culture.¹³⁻¹⁵ Also, manipulating liquid marble on water instead of a solid substrate increases the lifetime of the marble as the high humidity close to the liquid surface reduces the evaporation rate. The evaporation rates of a liquid marble in different environments¹⁶ and coating materials¹⁷ have been studied.

The present paper extends the research on liquid marbles into the realm of floating objects. A rigid spherical particle floating on a liquid deforms the liquid surface. However, in the case of a floating liquid marble, both the marble and the liquid surface deform. In this paper, we first discuss the existing theoretical models describing a floating solid sphere and then propose a floating oblate liquid spheroid model using well-

established governing equations. We will then use the proposed model to describe the deformation in terms of marble height and aspect ratio. The models are then compared to experimental data followed by detailed discussions.

2. Theoretical Background

Liquid marbles deform under gravity when resting on a solid surface.^{18, 19} Recently we investigated the deformation of a ferrofluid on a solid surface under the effect of magnetic force.¹⁸ Since gravitation force is negligible compared to surface tension at the small scale, magnetic force can work against the effect of surface tension and deforms a ferrofluid marble. Without the additional force such as magnetic force, a small liquid marble will take a spherical shape on a solid surface. However, the deformation will be different if the surface is a liquid surface that can also deform. Also, the deformation can be affected by the hydrophobicity of the coating material.²⁰ In this paper the hydrophobicity is one of the controlled variables, as only one type of coating powder is used. The height and contact radius used in previous works^{18, 19} can no longer describe the deformation. In the present work, we identify and redefine these parameters to describe the deformation of a floating liquid marble.

2.1 Floating solid sphere model

A floating spherical particle is a well-known problem with extensive past research,^{2, 21-29} which is hereby referred to as the solid model. Although immiscible floating liquid droplet has been investigated,³⁰⁻³¹ the liquid marble can be characterised using the solid model because the hydrophobic particle coating resembles a non-wetting soft surface.

Fig. 1 shows the key parameters of a floating spherical particle. To describe this floating particle, we need to obtain a unique set of solutions to all geometric parameters with a given set of intrinsic parameters of marble shape.

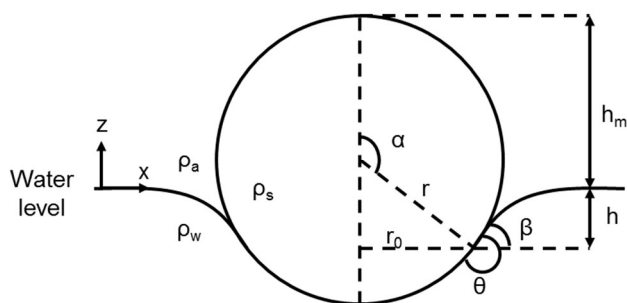


Fig. 1 Schematic of a floating particle with key parameters.

The intrinsic parameters are the densities of air ρ_a , carrier liquid ρ_w , marble liquid ρ_s , the surface tension between air and carrier liquid γ_w , the effective surface tension between the liquid marble and air γ_s the contact angle θ , the gravitational acceleration g , the capillary length $L_w = \sqrt{\gamma_w / (\rho_w - \rho_a)g}$ and

the Bond number of the liquid marble $Bo = \rho_s g r^2 / \gamma_s$. The geometric parameters are the radius of the undeformed spherical liquid marble r , the meniscus height h , the meniscus angle β , the contact radius r_0 and the three-phase contact position α .

The liquid marble is assumed to be a sphere with a known volume V , therefore the undeformed radius can be found as $r = \sqrt[3]{3V/4\pi}$. The meniscus angle is related to the contact angle and the three-phase contact position via trigonometric analysis, $\beta = \theta - \alpha$. Similarly, the contact radius is $r_0 = r \sin \alpha$. The remaining unknowns h and α are determined by simultaneously solving two governing equations.

For a floating body, the generalised Archimedes principle yields a force balance equation $F_w = F_s + F_B$, where F_w is the weight of the floating body, F_s is the surface tension force and F_B is the buoyancy force. This first governing equation is rewritten to explicitly express the meniscus height, h .^{2, 22, 23, 26, 28, 29, 32}

$$h = \left[\frac{(\rho_s - \rho_a) \frac{4}{3} \pi r^3 g - 2\pi \gamma_w \sin \alpha \sin \beta}{(\rho_w - \rho_a) \pi r^3 g} - \frac{2 + 3 \cos \alpha - \cos^3 \alpha}{3} \right] \left(\frac{r}{\sin^2 \alpha} \right) \quad (1)$$

Since the density of most liquids is much larger than that of air $\rho_s, \rho_w \gg \rho_a$, the above equation is further simplified to:

$$h = \left[\frac{\frac{4}{3} \rho_s r^2 g - 2\gamma_w \sin \alpha \sin \beta}{\rho_w r^2 g} - \frac{2 + 3 \cos \alpha - \cos^3 \alpha}{3} \right] \left(\frac{r}{\sin^2 \alpha} \right) \quad (2)$$

The second governing equation is the solution to the meniscus height using the Young-Laplace equation in its axisymmetric form:

$$\rho_w g z = \gamma_w \left[\frac{z_{xx}}{(1 + z_x^2)^{3/2}} + \frac{z_x}{x(1 + z_x^2)^{1/2}} \right] \quad (3)$$

Equation (3) does not have an exact, closed analytical solution.³³ This equation can only be solved using numerical methods^{2, 27-29, 31, 34, 35} or analytical approximation.^{26, 33, 36, 37} In our case, we use the analytical and empirical approximation methods developed by Nguyen.²⁶ For liquid marbles with a small contact radius, $r_0/L_w \leq 0.2$, the Derjaguin method³⁵ is used. For liquid marbles with a medium contact radius, $0.2 \leq r_0/L_w \leq 2$, Nguyen's empirical method²⁴ is used. This allows us to arrive at a closed analytical solution, which is convenient for trend analysis. Comparing to the numerical model, this empirical model is accurate if the meniscus angle is small, $\beta < \pi/2$.²⁶ Since we use small liquid marbles behaving like a superhydrophobic droplet, this condition is always satisfied. A superhydrophobic object is an object that has very large contact angle (typically $>150^\circ$) and practically non-wetting. The equations to determine h for liquid marbles of different sizes are as follow:

For a small contact radius, $r_0/L_w \leq 0.2$:

$$h = r_0 \sin \beta \left[\ln \frac{4L_w/r_0}{1 + \cos \beta} - C_{EM} \right] \quad (4)$$

where $C_{EM} = 0.5772\dots$ is the Euler-Mascheroni constant.

For a medium contact radius, $0.2 \leq r_0/L_w \leq 2$:

$$h = \frac{2.186L_w \sin \left[(0.5 + 0.322^{-2.122r_0/L_w}) \beta \right]}{1 + 0.649L_w/r_0} \quad (5)$$

The angle α can be solved by eliminating h . Subsequently, all the other unknown geometric parameters can be found. The numerical coefficients in equation (5) were determined empirically by Nguyen.²⁶

2.2 Floating oblate liquid spheroid model

The shape of a liquid marble resting on solid surface was accurately approximated using the oblate spheroid model.³⁸ The oblate spheroid is truncated at the liquid marble base as the solid surface does not deform. For our case, we approximate the floating liquid marble using two halves of an oblate spheroid with the same major axis but different minor axes. The two halves meet at the equator of the oblate spheroid so that the surface profile is always continuous. Let us also explore a hypothetical case where the liquid carrier is extremely viscous. The high viscosity will significantly restrict the ability of the bottom half of the liquid marble to deform. However, the top half is still exposed to air and generally unaffected. Therefore, we expect the two minor axes of the oblate spheroid halves to be different. This model serves as a convenient approximation tool to extract parameters needed to describe and compare the deformation to similar models. Fig. 2 illustrates the floating oblate liquid spheroid model.

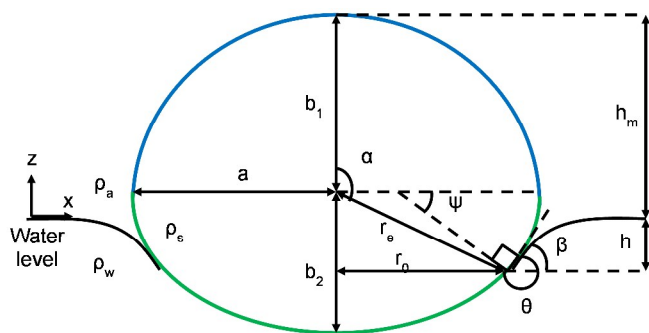


Fig. 2 Schematic of a floating oblate liquid spheroid with key parameters. The top half is in blue while the bottom half is in green.

As this model is a departure from the solid spherical particle, the theory has to be modified. Firstly, the meniscus angle is changed to $\beta = \theta - (\psi + \pi/2)$ where $\psi = \arctan \left[(a/b_2)^2 \tan(\alpha - \pi/2) \right]$. Similarly, the contact radius is $r_0 = r_e \sin \alpha$ where r_e is the distance from the equatorial centre to the three-phase contact position. r_e can be determined

from ellipsoidal geometry $r_e = ab_2 / \sqrt{(a \cos \alpha)^2 + (b_2 \sin \alpha)^2}$ where a and b_2 are the major and minor axes respectively. We assume that superhydrophobic liquid marbles invariably have three-phase contact positions under the equator. Therefore both ψ and r_e are dependent on b_2 instead of b_1 while α is always greater than $\pi/2$.

Following the ellipsoidal geometry, the volume of the liquid marble is:

$$V = \frac{4}{3} \pi r^3 = \frac{2}{3} \pi a^2 (b_1 + b_2) \quad (6)$$

Similar to the analysis of Wang and Yu³⁹ on an oblate spheroid surface profile, the minor axis b_1 can be related to the major axis as a function of the capillary length of the liquid marble, $L_s = \sqrt{\gamma_s / \rho_s g}$.³⁹ The curvature at the upper apex and the equator of the oblate spheroid are $2b_1/a^2$ and $1/a + a/b_1^2$ respectively. Therefore, the difference in Laplace pressure between these two points can be written as:

$$\rho_s g b_1 = \gamma_s \left(\frac{1}{a} + \frac{a}{b_1^2} - \frac{2b_1}{a^2} \right) \therefore L_s = \left(\frac{1}{ab_1} + \frac{a}{b_1^3} - \frac{2}{a^2} \right)^{-1/2} \quad (7)$$

An immediate outcome of the above equation is that the capillary length of the liquid marble can be determined simply by measuring the major and minor axes of the top half of the floating liquid marble. This method serves conveniently as an accurate measurement of the density and surface tension of the liquid marble. Conversely, if the volume and capillary length of the liquid marble are known, both minor axes b_1 and b_2 can be written as a function of a .

Equation (2) now has the form:

$$h = \frac{1}{r_0^2} \left\{ \frac{2\rho_s}{3\rho_w} a^2 (b_1 + b_2) - 2L_s^2 r_0 \sin \beta - \frac{a^2 b_2}{3} (1 + \cos \alpha)^2 (2 - \cos \alpha) \right\} \quad (8)$$

Since the variables b_1 and b_2 can be eliminated using the volume and Laplace pressure equation, h only has two independent variables, a and α . By equating (8) with (4) or (5), α can then be eliminated as well. Therefore, only a needs to be measured to obtain a unique solution for the floating oblate liquid spheroid model.

A more comprehensive, numerical approach is to break down the system into three fluid profiles: the non-submerged section of the marble f_1 , the submerged section f_3 and the semi-infinite meniscus section f_2 . The volume of the marble is similarly split into two sections: the non-submerged (V_1) and submerged section (V_2), where $V = V_1 + V_2$. V_3 is the cylindrical volume contained within V_1 . These parameters are shown in Figure 3.

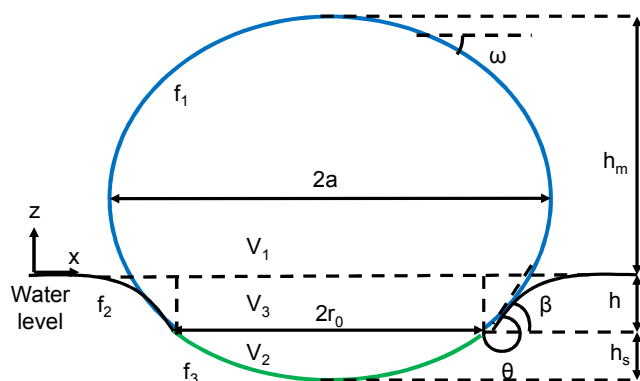


Fig. 3 Schematic of the numerical approach with key parameters indicated.

The Young-Laplace equation can be solved numerically in its popular parametric form. For an axisymmetric profile, the arc length s and the inclination of the profile at any point ω are introduced. We then obtain the following set of equations:

$$\frac{d\omega}{ds} = \frac{2}{u} + \frac{\rho_w g z}{\gamma_w} - \frac{\sin \omega}{x}, \quad \frac{dx}{ds} = \cos \omega, \quad \frac{dz}{ds} = \sin \omega \quad (9)$$

where u is the curvature at the initial position defined by the x - z coordinate system. For f_1 and f_3 , this curvature is at the top and bottom apexes of the marble, respectively. For f_2 , the curvature is at the water level position. The three fluid profiles can be solved individually using the Young-Laplace equation if the required boundary conditions are known. For f_1 , the top apex curvature and final ω position need to be known. For f_2 , both r_0 and β need to be known. The submerged profile f_3 can only be solved if the bottom apex curvature, final ω position and the entire profile f_1 are known. Since our present work aims to develop a quick approximation to describe the deformation, the exact solution that involves solving a complex system of differential equations will be implemented in future works.

3. Materials and Methods

The liquid marble was prepared by rolling a droplet of deionised (DI) water on a bed of polytetrafluoroethylene (PTFE) powder. The liquid marble is completely coated before being transferred onto a non-coated surface. The liquid marble is then allowed to roll around to remove excessive coating and increase coating uniformity across liquid marbles. Droplets of different volumes were dispensed using a micropipette to ensure high accuracy. The PTFE powder was supplied by Sigma-Aldrich with a nominal diameter of 1 μm and density of approximately 2,200 kg/m^3 . A clear polystyrene (PS) container was used to minimise the meniscus climb of water on the container wall, as recommended by Extrand and Moon.²³ In our case, the carrier liquid is DI water with a density of 1,000 kg/m^3 and surface tension of 0.072 N/m.

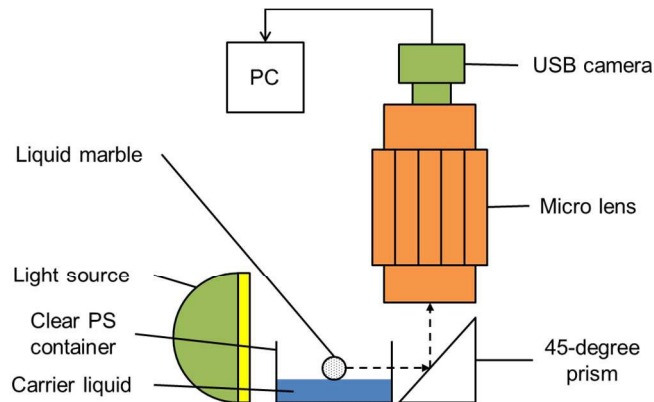
The effective surface tension of the liquid marble can be found using the puddle height method $\gamma_s = h_p^2 \rho_s g / 4$,¹⁸ where h_p is the height of a large liquid marble with a puddle shape resting on a solid substrate. In our case, the effective surface tension of the liquid marble was determined as 0.068 N/m, similar to measurements done by Arbatan and Shen where the same materials were used.⁴⁰ The density of liquid marble is assumed to be the same as DI water because the weight of the coating powder is several orders of magnitude smaller than that of the encapsulated liquid. These properties will be used for theoretical calculations. The true effective surface tension and density of the liquid marble are much more difficult to measure. It is known that the effective surface tension varies with volume, as shown by Bormashenko *et al.*⁴¹ In his work, the pendant method measurement of the effective surface tension was further complicated by inflation and deflation hysteresis. For our case, this is less apparent as the puddle height method does not involve liquid addition or removal. Likewise, the actual density of the liquid marble is complicated by the fact that the coating is a non-uniform, multi-layered, and aggregated particles with air pockets in it. This causes theoretical calculations to consistently overestimate the actual density of the liquid marble.

Our inability to accurately measure both effective surface tension on water and density of the liquid marble contributes to the error in the capillary length L_s , which is used to describe $b_l(a)$. Moreover, the solid fraction of the coating affects the effective surface tension of the floating liquid marble.⁴² We were not able to ensure the consistency of the solid fraction as the loose powder forms aggregate of random sizes. Nonetheless a consistent procedure was implemented during marble preparation to minimize variation of the coating condition across liquid marbles. Additionally, we measure both a and b_l to determine L_s , which contain both the effective surface tension and density of the liquid marble. This measurement is done for individual floating liquid marble to address the variation in terms of volume and carrier type. Consequently we are able to determine the error in L_s for our results analysis. Table 1 shows parameters that are either measured or calculated for theoretical models and experimental results.

Table 1. Parameters used for theoretical models and experimental results.

Parameters	Floating solid sphere	Floating oblate liquid spheroid	Experimental results	
Capillary length of the liquid carrier	L_w	2.71 mm	2.71 mm	Not required
Capillary length of floating the liquid marble	L_s	Not required	2.63 mm	Calculated from measurements of a and b_1
Major axis of oblate spheroid	a	Calculated. $a = r$	Measured	Measured
Upper minor axis of oblate spheroid	b_1	$b_1 = a$	Calculated	Measured
Lower minor axis of oblate spheroid	b_2	$b_2 = a$	Calculated	Measured
Height of liquid marble above water level	h_m	Calculated	Calculated	Measured
Liquid marble contact radius	r_0	Calculated	Calculated	Not required

The liquid marble was backlit with a light source. A USB camera (Edmund Optics) captures the side view via a 45-degree prism and a Nikon 60 mm f2.8 microlens. The image was then recorded by the camera and sent to the PC for data analysis. All data analysis and measurements were done using ImageJ (NIH, USA). Fig. 4 shows the experimental setup. The container is partially filled with some DI water prior to the placement of the liquid marble. After the placement, additional water is slowly added into the container to produce a consistent advancing contact angle at the container wall. Due to evaporation, the volume of the liquid marble is transient in nature. Additionally, significant reduction in marble volume will result in a higher particle fraction of the coating. Therefore, the entire process of liquid marble preparation to the final image acquisition was conducted with a total duration of less than 5 minutes to reduce this effect. Since the liquid marble spends most of its time floating on water, the high relative humidity of its environment serves to reduce its evaporation rate.¹⁶ Therefore, the liquid marble volume is assumed to be constant throughout the experiment. Throughout the short duration of the experiment, the liquid marble shape appears stable, hence the viscoelastic effects of the liquid marble coating are assumed to be negligible for this case. None of the liquid marble burst within minutes after proper placement on water, unlike previous reports.¹⁷ The stability is most likely due to a difference in PTFE diameters as the powder used in the experiment is smaller than that of previous report, 1 μm compared to 7 μm .

**Fig. 4** The experimental setup. The dashed lines indicate the optical path.

4. Results and discussions

Fig. 5 shows an example of the side view of a floating liquid marble. The small marble only creates a slight depression on the water surface. The PTFE coating makes a very large, constant contact angle with the carrier liquid, $\theta \approx \pi$ in agreement with previous reports,⁴³ because air is present between the liquid marble and the liquid carrier. This fact can also be verified with the smooth and continuous meniscus profile at the three-phase contact point. These two factors caused the three phase contact point to be obstructed by the meniscus, preventing accurate measurements of r_0 and a . Therefore, we measured the height of the marble above the water level h_m , the major axis a , minor axes b_1 , and b_2 for the analysis.

Minor surface cracks are observed on the liquid marbles, as shown in Figure 5. These cracks could be an indicator that the surface tension is not uniform across the liquid marble, similar to Vella's finding on particle rafts.⁴⁴ They can also form due to the different surface area of the liquid marble being coated on a solid surface and then transferred to a liquid surface. The floating liquid marble deforms more, resulting in a larger surface area. This effectively creates a deficit in the coating layer, resulting in minor cracks.

We hypothesise that there is a difference in effective surface tensions between the interface where the liquid marble meets the air and the interface where the liquid marble meets the liquid carrier. This is because the particle coating is sandwiched between two different fluids at different locations on the liquid marble. This affects the local particle distribution which leads to different effective surface tensions. This difference is not covered in this paper, but it is an important consideration as the local effective surface tension could influence the collapse mechanism.

The transient aspect of the deformation is not covered in this paper due to the limitations of the experimental method. The liquid marble was rolled onto water surface and allowed to come to a complete stop. Furthermore, the marble was allowed to rest for several minutes before the measurement.

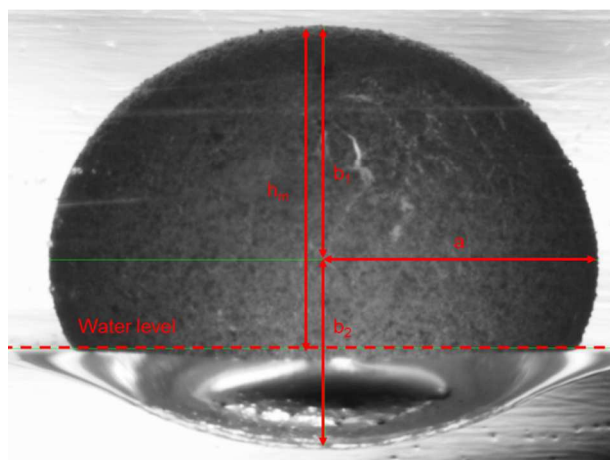


Fig. 5 Side view of a floating liquid marble on water. The liquid marble appears dark because it is backlit. Red lines are superimposed on the photograph to indicate measured parameters.

From Figures 1, 2 and 5, the water level is the non-deformed surface of the carrier liquid sufficiently far away from the marble. The maximum equatorial width of the marble is measured. Half of this width is the major axis, a . From the centre of the maximum width, the minor axes b_1 and b_2 are measured towards the top and bottom apices respectively. The height h_m is measured from the water level to the top apex of the marble. We measured all these parameters for marble volumes 1, 2, 5, 10, 20 and 50 μl . The height h_m is then normalised by the radius of the undeformed spherical marble to yield $h_m^* = h_m / r$. Theoretical values for the same set of volume are calculated as well, using the simple relationship $h_m = b_1 - r_e \cos \alpha - h$. These values are plotted in the same graph as shown in Figure 6(a).

Figure 6(a) shows lines that indicate different theoretical models. The dotted line represents a non-deformable floating solid sphere model while the solid line represents the floating oblate liquid spheroid model. Vertical error bars indicate a 90% confidence interval on the measurement of the marble height. Horizontal error bars indicate a 90% confidence interval on the combined uncertainties that arise from the effective surface tension and density of the liquid marble. It is apparent that the experimental data are somewhere in between a floating solid sphere and an oblate liquid spheroid. The density and effective surface tension of the liquid marble are 1,000 kg/m^3 and 0.068 N/m respectively. This yields a capillary length of $L_s = 2.63$

mm which is assumed to be constant. The experimental values showed consistently larger capillary lengths than 2.63 mm as used by the theoretical model, as calculated from the measurements of a and b_1 shown in Table 1. The experimental capillary lengths ranged from 2.63 mm to 3.10 mm.

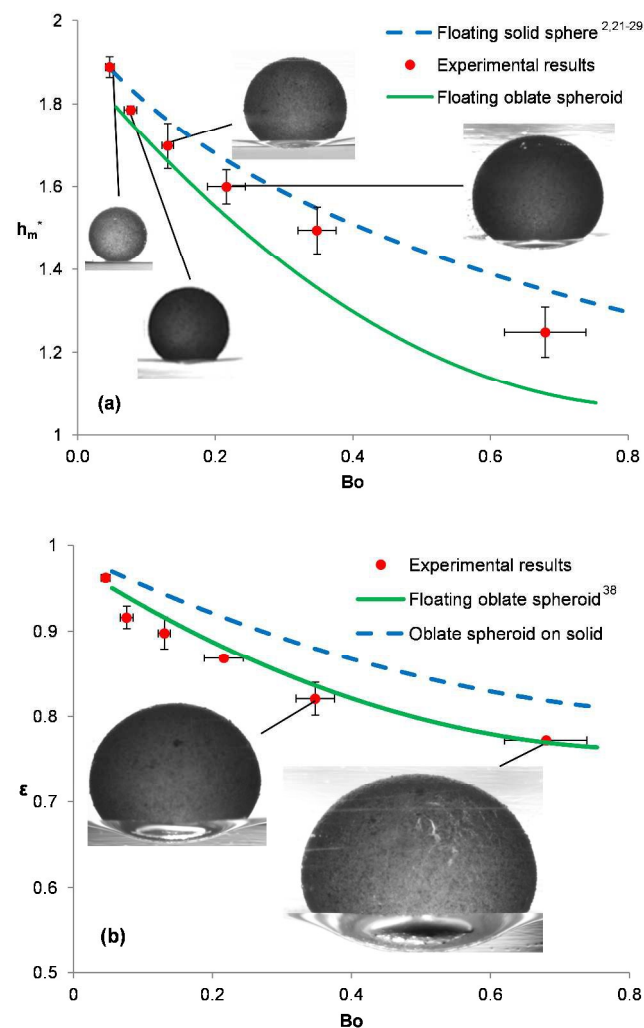


Fig. 6 Experimental and theoretical data of the side view of floating liquid marbles: (a) Dimensionless height of the marble above water level h_m^* versus Bond number. (b) Aspect ratio $\epsilon = (b_1 + b_2)/2a$ versus Bond number. All error bars indicate a 90% confidence interval.

This is likely due to trapped air pockets in the coating and unpredictable surface gap filling mechanisms as explained in detail by Bormashenko *et al.*⁴¹ If the effective surface tension is taken to be infinitely large, $\lim \gamma_s \rightarrow \infty$, the Bond number will reduce to zero. The liquid marble is then essentially a solid sphere without any deformation and yield the specific case of $b_2 = b_1 = a = r$. Substituting this into equation (8) will also lead to equation (2). Graphically, the solid line will converge with the dotted line in Figure 6(a) and the floating liquid marble then effectively becomes a floating solid sphere. Both floating solid

and oblate liquid spheroid models serve very well as theoretical upper and lower bounds respectively.

Next, the deformation of the floating liquid marble is investigated in terms of its aspect ratio. We take the total height of the divided by the maximum width of the marble to be its aspect ratio, $\varepsilon = (b_1 + b_2)/2a$. The solid model assumes zero deformation, which means that the aspect ratio is always equal to unity. Therefore, this model is irrelevant in the discussion of the deformation of the floating marble. Instead, the deformation is compared to that of a sessile liquid marble on a solid surface. Using an oblate spheroid model and energy minimisation method, Whyman and Bormashenko accurately approximated the profile of the sessile droplet.³⁸ The theoretical results obtained using their model are plotted as the dotted line in Figure 6(b), labelled as oblate spheroid on solid. The values calculated using the floating oblate spheroid model are plotted as a solid line. Figure 6(b) shows that our current model much better approximates the experimental data, as the floating oblate spheroid model takes into account the difference in the upper and lower minor axes, which is clearly illustrated in Figure 6.

Alternatively from an energy analysis approach, the liquid marble gains surface energy to deform itself from the loss of potential energy. For a floating liquid marble, the potential energy loss is more than one resting on a solid surface because it is allowed to partially sink into the liquid carrier. Here we show that even after expending energy for potential and surface energy gain of the liquid carrier, the floating liquid marble still possesses sufficient surface energy to deform itself to a significant extent. The energy analysis approach is more general and computationally demanding, but it could shed more insight on energy partitioning of the entire system.

The imperfections of the container wall surface enlarge the advancing contact angle between water and PS surface. The water level is then depressed, inflating the h_m reading. This is why the results in Figure 6(b) are more accurate than 6(a), since the aspect ratio of the liquid marble is not affected by the error in h_m .

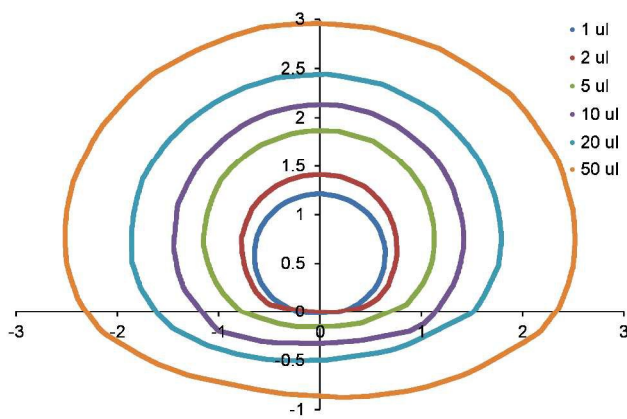


Fig. 7 Outlines of liquid marbles with different volumes extracted from experimental data depicted as inserts in Figure 6 (a) and (b). The horizontal axis represents the water level, the vertical axis represents the height of the marble. Both axes are in mm.

5. Conclusion

This paper shows that the deformation of the liquid marble can be characterised by the floating oblate spheroid model, which is a generalisation of the well-established floating solid sphere model. The model assumes that the floating liquid marble forms two halves of an oblate spheroid conjoined at the equator. Ellipsoidal geometry is used in conjunction with generalised Archimedes principle and analytical approximations to the Young-Laplace equation.

In terms of height of the liquid marble above the water level, the experimental data lie between a floating solid and an oblate liquid spheroid. The errors are caused by uncertainties in the effective capillary length of the liquid marble and surface imperfections of the container wall. In terms of the aspect ratio of the liquid marble, the floating oblate liquid spheroid well approximates the experimental results. The deformation of a floating marble is clearly different than that of a sessile marble resting on solid surface.

Knowledge of the deformation of the floating liquid marble allows us to better approximate the evaporation rate, as current theoretical evaporation models are based on sessile droplets on solid flat surfaces. We hypothesise that the floating liquid marble has a different surface area exposed to air and relative humidity.

Liquid marbles placed on solid surface are known to evaporate and eventually collapse.¹⁶ Floating liquid marbles collapse as well, releasing its content into the liquid carrier. The mechanism of its collapse warrants further study. Preliminary trials indicate that floating liquid marble can last up to several days in a humid environment. It has a longer lifetime compared to that of a liquid marble on solid surface due to its proximity to water, which is a desirable feature for cell culture applications. As the liquid marble coating is porous, there is an exchange of water molecules between the liquid marble and the liquid carrier at close range. Further investigation is needed to determine whether the increased relative humidity or difference in surface area is the major contributing factor.

With the proposed floating oblate spheroid model, the surface area exposed or submerged can be described with a convenient analytical expression. Consequently, the lifetime and the stability of the liquid marble can be characterised. The rate of air exchange that is crucial for biological content of the marble can then be studied as well. Furthermore, the deformation of the liquid marble can form a basis to the study

on the maximum Bond number of a liquid marble that can remain buoyant. This allows the determination of the payload of any liquid marble on a liquid carrier and subsequently the mechanism of its actuation scheme.

Acknowledgements

We acknowledge Queensland Micro- and Nanotechnology Centre for providing the facilities to make the experiments possible. NTN acknowledges funding support from Griffith University through a start-up grant and a grant from the Griffith University Research Infrastructure Program (GURIP). CHO and RV are supported through Griffith Sciences and the Griffith University International Postgraduate Research Scholarships (GUIPRS), respectively.

Notes and references

^a Queensland Micro- and Nanotechnology Centre, Griffith University, 170 Kessels Road, 4111 Queensland, Australia.

^b Eskitis Institute for Drug Discovery, Griffith University, 170 Kessels Road, 4111 Queensland, Australia.

* email: nam-trung.nguyen@griffith.edu.au

† Footnotes should appear here. These might include comments relevant to but not central to the matter under discussion, limited experimental and spectral data, and crystallographic data.

Electronic Supplementary Information (ESI) available: [details of any supplementary information available should be included here]. See DOI: 10.1039/b000000x/

References

1. E. Bormashenko, Y. Bormashenko and A. Musin, *J Colloid Interface Sci*, 2009, **333**, 419-421.
2. D. Vella, D. G. Lee and H. Y. Kim, *Langmuir : the ACS journal of surfaces and colloids*, 2006, **22**, 5979-5981.
3. E. Bormashenko and A. Musin, *Applied Surface Science*, 2009, **255**, 6429-6431.
4. E. Bormashenko, Y. Bormashenko, A. Musin and Z. Barkay, *Chemphyschem : a European journal of chemical physics and physical chemistry*, 2009, **10**, 654-656.
5. Y. Couder, E. Fort, C. H. Gautier and A. Boudaoud, *Physical Review Letters*, 2005, **94**, 177801.
6. A. B. D. Cassie and S. Baxter, *Transactions of the Faraday Society*, 1944, **40**, 546-551.
7. C. W. Extrand, *Langmuir : the ACS journal of surfaces and colloids*, 2002, **18**, 7991-7999.
8. D. Dupin, S. P. Armes and S. Fujii, *Journal of the American Chemical Society*, 2009, **131**, 5386-5387.
9. S. Fujii, M. Suzuki, S. P. Armes, D. Dupin, S. Hamasaki, K. Aono and Y. Nakamura, *Langmuir : the ACS journal of surfaces and colloids*, 2011, **27**, 8067-8074.
10. L. Gao and T. J. McCarthy, *Langmuir : the ACS journal of surfaces and colloids*, 2007, **23**, 10445-10447.
11. L. Zhang, D. Cha and P. Wang, *Advanced Materials*, 2012, **24**, 4756-4760.
12. E. Bormashenko, R. Pogreb and A. Musin, *Journal of Colloid and Interface Science*, 2012, **366**, 196-199.
13. T. Arbatan, A. Al-Abboodi, F. Sarvi, P. P. Chan and W. Shen, *Advanced healthcare materials*, 2012, **1**, 467-469.
14. F. Sarvi, K. Jain, T. Arbatan, P. J. Verma, K. Hourigan, M. C. Thompson, W. Shen and P. P. Y. Chan, *Advanced healthcare materials*, 2014, n/a-n/a.
15. J. Tian, N. Fu, X. D. Chen and W. Shen, *Colloids and Surfaces B: Biointerfaces*, 2013, **106**, 187-190.
16. A. Tosun and H. Y. Erbil, *Applied Surface Science*, 2009, **256**, 1278-1283.
17. U. Cengiz and H. Y. Erbil, *Soft Matter*, 2013, **9**, 8980-8991.
18. P. Aussillous and D. Quere, *P Roy Soc a-Math Phy*, 2006, **462**, 973-999.
19. L. Mahadevan and Y. Pomeau, *Phys Fluids*, 1999, **11**, 2449-2453.
20. D. Zang, Z. Chen, Y. Zhang, K. Lin, X. Geng and B. P. Binks, *Soft Matter*, 2013, **9**, 5067.
21. I. B. Ivanov, P. A. Kralchevsky and A. D. Nikolov, *Journal of Colloid and Interface Science*, 1986, **112**, 97-107.
22. C. W. Extrand and S. I. Moon, *Langmuir : the ACS journal of surfaces and colloids*, 2008, **25**, 992-996.
23. C. W. Extrand and S. I. Moon, *Langmuir : the ACS journal of surfaces and colloids*, 2009, **25**, 6239-6244.
24. J. B. Keller, *Physics of Fluids (1994-present)*, 1998, **10**, 3009-3010.
25. X. Liu, X. Wang, Y. Liang and F. Zhou, *J Colloid Interface Sci*, 2009, **336**, 743-749.
26. A. V. Nguyen, *Journal of Colloid and Interface Science*, 2002, **249**, 147-151.
27. C. Pozrikidis, *Journal of Colloid and Interface Science*, 2011, **364**, 248-256.
28. D. Vella, Ph.D. Thesis, University of Cambridge, 2007.
29. C. Huh and L. E. Scriven, *Journal of Colloid and Interface Science*, 1969, **30**, 323-337.
30. C. M. Phan, *Langmuir : the ACS journal of surfaces and colloids*, 2014, **30**, 768-773.
31. R. Shabani, R. Kumar and H. J. Cho, *Appl Phys Lett*, 2013, **102**, -.
32. H. J. Schulze, *Physio-chemical elementary processes in flotation*, Elsevier, Amsterdam, 1984.
33. P. A. Kralchevsky, K. D. Danov and N. D. Denkov, in *Handbook of Surface and Colloid Chemistry*, ed. K. S. Birdi, Taylor and Francis Group, 3rd edn., 2009, ch. 7, pp. 197-355.
34. A. R. Alois and A. F. Rincón, *Revista Colombiana de Química*, 2010, **39**, 413-425.
35. F. Bashforth and J. C. Adams, *An attempt to test the theories of capillary action by comparing the theoretical and measured forms of drops of fluid.*, Cambridge University Press, 1883.
36. P. A. Kralchevsky, I. B. Ivanov and A. D. Nikolov, *Journal of Colloid and Interface Science*, 1986, **112**, 108-121.
37. B. V. Derjaguin, *Dokl. Akad. Nauk USSR*, 1946, **51**, 517.
38. G. Whyman and E. Bormashenko, *Journal of Colloid and Interface Science*, 2009, **331**, 174-177.
39. X. Wang and Y. Yu, *Sci. China Phys. Mech. Astron.*, 2012, **55**, 1118-1124.
40. T. Arbatan and W. Shen, *Langmuir : the ACS journal of surfaces and colloids*, 2011, **27**, 12923-12929.

41. E. Bormashenko, A. Musin, G. Whyman, Z. Barkay, A. Starostin, V. Valtsifer and V. Strelnikov, *Colloids and Surfaces A: Physicochemical and Engineering Aspects*, 2013, **425**, 15-23.
42. C. Monteux, J. Kirkwood, H. Xu, E. Jung and G. G. Fuller, *Physical Chemistry Chemical Physics*, 2007, **9**, 6344-6350.
43. P. Aussillous and D. Quere, *Nature*, 2001, **411**, 924-927.
44. D. Vella, P. Aussillous and L. Mahadevan, *Europhysics Letters (EPL)*, 2004, **68**, 212-218.